

# CHEMISTRY

## A European Journal

A Journal of



### Accepted Article

**Title:** Phosphorescence Tuning via Heavy Atom Placement in Unsymmetrical Difluoroboron b-Diketonate Materials

**Authors:** Tiandong Liu, Guoqing Zhang, Ruffin Evans, Carl Trindle, Zikri Altun, Christopher DeRosa, Fang Wang, Meng Zhuang, and Cassandra L. Fraser

This manuscript has been accepted after peer review and appears as an Accepted Article online prior to editing, proofing, and formal publication of the final Version of Record (VoR). This work is currently citable by using the Digital Object Identifier (DOI) given below. The VoR will be published online in Early View as soon as possible and may be different to this Accepted Article as a result of editing. Readers should obtain the VoR from the journal website shown below when it is published to ensure accuracy of information. The authors are responsible for the content of this Accepted Article.

**To be cited as:** *Chem. Eur. J.* 10.1002/chem.201703513

**Link to VoR:** <http://dx.doi.org/10.1002/chem.201703513>

Supported by  
**ACES**

WILEY-VCH

# Phosphorescence Tuning via Heavy Atom Placement in Unsymmetrical Difluoroboron $\beta$ -Diketonate Materials

Tiandong Liu,<sup>[a]</sup> Guoqing Zhang,<sup>[a,b]</sup> Ruffin E. Evans,<sup>[a,c]</sup> Carl O. Trindle,<sup>[a]</sup> Zikri Altun,<sup>[d]</sup> Christopher A. DeRosa,<sup>[a]</sup> Fang Wang,<sup>[a]</sup> Meng Zhuang,<sup>[a]</sup> and Cassandra L. Fraser<sup>\*[a]</sup>

**Abstract:** Difluoroboron  $\beta$ -diketonates (BF<sub>2</sub>bdks) show both fluorescence (F) and room-temperature phosphorescence (RTP) when confined to a rigid matrix such as poly(lactic acid). These materials have been utilized as optical oxygen sensors (e.g. tumors, wounds and cells). Spectra features include charge transfer (CT) from the major aromatic donor to the bdk acceptor. A series of naphthyl-phenyl dyes (BF<sub>2</sub>nbm) (**1-6**) were prepared to test heavy-atom placement effects. The BF<sub>2</sub>nbm dye (**1**) was substituted with Br on naphthyl (**2**), phenyl (**3**), or both rings (**4**) to tailor the F/P ratio and RTP lifetime—important features for designing O<sub>2</sub> sensing dyes via the heavy atom effect. Computational studies identify the naphthyl ring as the major donor. Thus, Br substitution on the naphthyl ring produced greater effects on the optical properties such as increased RTP intensity and decreased RTP lifetime compared to phenyl substitution. However, for electron-donating piperidyl-phenyl dyes (**5**), the phenyl aromatic is the major donor. As a result, Br substitution on the naphthyl ring (**6**) did not alter the optical properties significantly. Experimental data and computational modelling show the importance of Br position. The S<sub>1</sub> and T<sub>1</sub> states are described by two singly occupied MOs (SOMOs). When both of these SOMOs have substantial amplitude on the heavy atom, passage from S<sub>1</sub> to T<sub>1</sub> and emission from T<sub>1</sub> to S<sub>0</sub> are both favoured. This shortens the excited state lifetimes and enhances phosphorescence.

## Introduction

Phosphorescence emission has garnered much interest over the years, particularly for light emitting diode (LED) applications and optical oxygen sensing.<sup>1-3</sup> Recently, organic compounds have attracted renewed interest as alternatives to metal-activated phosphors and inorganic salts. However, organic materials that show phosphorescence are typically very sensitive to oxygen.<sup>4</sup> Some organic materials only phosphoresce

when confined to a rigid matrix, such as a crystal, where the dyes are “shielded” from collisional quenching by oxygen.<sup>5,6</sup> Notably, dyes such as difluoroboron diketonates (BF<sub>2</sub>bdks) show both fluorescence and phosphorescence at room temperature when embedded into a rigid polymer, such as poly(lactic acid) (PLA). When exposed to air, the phosphorescence is completely quenched, but the fluorescence is unaffected.<sup>7</sup> Such phenomena have been exploited for ratiometric oxygen sensing.<sup>8,9</sup>

Previous reports established that when difluoroboron dibenzoylmethane (BF<sub>2</sub>dbm) was embedded in poly(lactic acid), whether covalently attached or blended, it exhibited room temperature phosphorescence (RTP) in addition to intense fluorescence.<sup>7,10</sup> Due to the long phosphorescence lifetime of the dye, and the permeability of oxygen through PLA, the RTP is highly sensitive to oxygen. Through nanoprecipitation methods, dual-emissive BF<sub>2</sub>bdkPLA materials can be converted into nanoparticles for use as ratiometric oxygen probes for in vivo hypoxia imaging.<sup>1,11-13</sup> Given the many benefits of BF<sub>2</sub>dbm triplet emission for oxygen sensing and imaging in biological contexts and other uses, it is important to develop systematic methods to tune both fluorescence and RTP, not just in the blue-green region but other wavelength ranges as well, for multiplexing and greater tissue penetration of light.<sup>14</sup> An important first step is to understand the nature of the excited states, which, for example, could be from intramolecular charge transfer or delocalized  $\pi - \pi^*$  states.<sup>15</sup> Recent investigations revealed that both  $\pi$ -conjugation and intramolecular charge transfer (ICT) contribute to the photophysical properties of the BF<sub>2</sub>bdk dyes.<sup>16-18</sup> When the two aryl groups of the diketone have identical or comparable electron donating abilities, the dye is prone to excitation through  $\pi - \pi^*$  transitions for the lowest excited state and its intrinsic fluorescence lifetime is typically short (~2 ns). If one of the aryls is replaced by a stronger donor, some ICT character in the transition can be expected. Increasing the disparity in electron donating ability of the two aromatic donors favors ICT character relative to a  $\pi - \pi^*$  transition, and the lifetime increases (e.g. anthryl-phenyl dye, BF<sub>2</sub>abm, in PLA:  $\tau = \sim 10$  ns).<sup>16</sup> Altering the influence of the ICT process could be an effective method to adjust emission properties, thereby achieving desired optical properties by tuning lifetimes and altering the fluorescence-to-phosphorescence ratio.

In this study, the heavy atom effect was employed as a tool to screen the modulation of the ICT process, particularly in triplet emission. Previous reports on this class of compounds covalently linked to PLA, not blended, revealed phosphorescence tunable by heavy atom placement and polymer molecular weight.<sup>19</sup> Here, we have designed a panel of six difluoroboron naphthoylbenzoylmethane complexes (BF<sub>2</sub>nbm), as shown in Figure 1, to study the influences of charge transfer and fluorescence to phosphorescence (F/P) ratio tuning in depth. To assess whether phosphorescence properties could be controlled by arene ring sizes and substituents,

[a] Carl O. Trindle, Christopher A. DeRosa, Fang Wang, Meng Zhuang, Cassandra L. Fraser\*  
Department of Chemistry  
University of Virginia  
McCormick Road, Charlottesville, VA 22904, USA  
E-mail: fraser@virginia.edu

[b] Guoqing Zhang  
Hefei National Laboratory for Physical Sciences at the Microscale  
University of Science and Technology of China  
Hefei, Anhui, 230026 China

[c] Ruffin Evans  
Department of Physics  
Harvard University  
Cambridge, MA 02138, USA

[d] Prof. Zikri Altun  
Department of Physics  
Marmara University Göztepe Kampusu  
Istanbul, Turkey, 34772

## FULL PAPER

WILEY-VCH

bromide and amine groups were attached on naphthyl or phenyl groups to modulate the electronic properties of the donor moieties. The rationale is as follows. In order to obtain strong phosphorescence, efficient passage from  $S_1 \rightarrow T_1$  and bright emission from  $T_1 \rightarrow S_0$  must both occur. A heavy atom is known to exert strong spin-orbit coupling. Triplet-singlet mixing is enhanced by strong spin-orbit coupling, a small singlet-triplet gap, and substantial amplitude at the heavy atom in both coupled SOMOs. Charge transfer transitions typically have small  $S_1-T_1$  energy gaps, so if the  $S_0-S_1$  transition has substantial charge transfer character, ISC to  $T_1$  can be enhanced.<sup>20,21</sup> Near unit ISC yield could be expected for an almost pure CT, and if emission from the  $T_1$  state is not rapid, delayed fluorescence is expected.<sup>22-24</sup> Both the CT character of the transition (which affects the first ISC process) and the impact of the placement of the heavy atom (which can influence both the first ISC and the rate of emission from  $T_1$ ) play roles in determining the total emission spectra. In this study, we combine experimental observation and computational characterization of states participating in the photophysics for  $BF_2$ bdk dyes **1-6**. To the best of our knowledge, no previous study has described the interplay of CT and heavy atom effects on emission spectra in this manner.

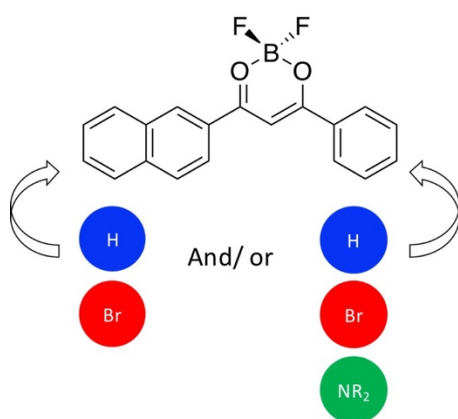
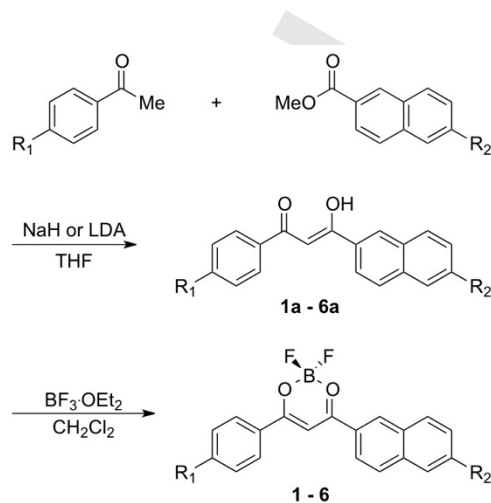


**Figure 1.** Chemical modifications to difluoroboron naphthyl-phenyl  $\beta$ -diketonate complexes.

## Results and Discussion

**Synthesis.** The  $\beta$ -diketonate ligands were prepared by Claisen condensation, shown in Scheme 1. The ketone precursors in **1a-4a** were deprotonated by NaH before reaction with the desired esters. In **5a** and **6a**, due to the existence of electron donating piperidine, which renders the ketone less acidic, a stronger base is required to facilitate the reaction. Using LDA, the ligands **5a** and **6a** were obtained in moderate yield. The boron compounds **1-6** were obtained from a previously reported method in moderate to good yields.<sup>16</sup> The boronation reaction was carried out with boron trifluoride etherate and the corresponding  $\beta$ -diketonates in dichloromethane. Immediately upon the addition of the boron reagent, intense fluorescence is observed. After ~2 h under refluxing, the ligand typically cannot be observed on thin-layer chromatography (TLC) plate and the reaction was considered complete. The yields were up to 70% after recrystallization or over 80% yield after column chromatography.

Dyes **1-4** are yellow solids and show intense fluorescence under UV light, however, luminescence from orange solids **5** and **6** is very weak and can barely be observed by the naked eye.



	$R_1$	$R_2$
<b>1</b> $BF_2nbm$	H	H
<b>2</b> $BF_2n(Br)bm$	H	Br
<b>3</b> $BF_2nb(Br)m$	Br	H
<b>4</b> $BF_2n(Br)b(Br)m$	Br	Br
<b>5</b> $BF_2nb(pip)m$	pip	H
<b>6</b> $BF_2n(Br)b(pip)m$	pip	Br

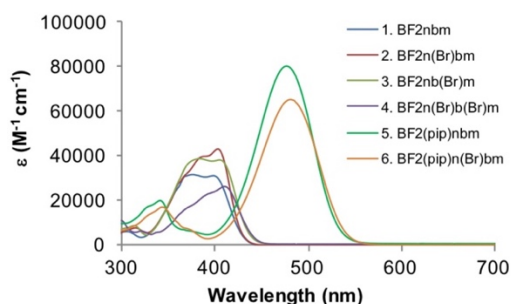
**Scheme 1.** Synthesis of Naphthyl-Phenyl  $\beta$ -Diketonate Ligands and Boron Complexes.

**Optical Properties in Solution.** The optical properties were measured in dilute  $CH_2Cl_2$  (Table 1). The absorption spectra of dyes **1-6** in  $CH_2Cl_2$  solution are shown in Figure 2. The absorption maxima of **1-4** range from 377-411 nm. Absorption maxima of  $BF_2nb(pip)m$  (**5**) and  $BF_2n(Br)b(pip)m$  (**6**) are at 477 and 482 nm respectively in addition to a small absorption peak at around 370 nm. The considerable bathochromic shifts of **5** and **6** in a polar solvent indicate an extended conjugation in the  $\pi$  system and a significant contribution from enhanced ICT to the transition.<sup>25-27</sup>

**Table 1.** Optical Properties of BF<sub>2</sub>nbm Complexes **1-6** in CH<sub>2</sub>Cl<sub>2</sub>

Sample	$\lambda_{\text{max}}^{[a]}$ (nm)	$\epsilon^{[b]}$ (M <sup>-1</sup> cm <sup>-1</sup> )	$\lambda_{\text{em}}^{[c]}$ (nm)	$\lambda_{\text{F}}^{[d]}$ (ns)	$\Phi_{\text{F}}^{[f]}$	$\tau_{\text{rad}}^{[g]}$ (ns)	Stokes Shift (cm <sup>-1</sup> )
<b>1</b>	377 <sup>[h]</sup>	37100	482	4.82	0.50	9.68	4320
	399	37900					
<b>2</b>	382 <sup>[h]</sup>	39000	460	0.86	0.17	5.06	2990
	403	42900					
<b>3</b>	383 <sup>[h]</sup>	39000	490	4.58	0.31	14.8	4280
	405	39000					
<b>4</b>	411 <sup>[i]</sup>	34000	465	0.80	0.18	4.44	2820
<b>5</b>	341 <sup>[h]</sup>	19600	444 <sup>[h]</sup>	1.42	0.025	44.0	6800
	477	80100	561	1.10			3140
<b>6</b>	344 <sup>[h]</sup>	16900	459 <sup>[h]</sup>	0.88	0.0093	300	7280
	482	65400	553	2.79 <sup>[e]</sup>			2660

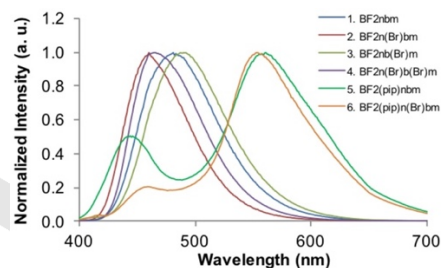
[a] Absorption maxima. [b] Extinction coefficients calculated at the absorption maxima. [c] Fluorescence emission maximum. [d] Fluorescence lifetime excited with a 369 nm LED monitored at the emission maxima. All fluorescence lifetimes are fitted with single-exponential decays unless indicated. [e] Double exponential decay. [f] Relative fluorescence quantum yield using quinine sulfate in 0.1M H<sub>2</sub>SO<sub>4</sub> as a standard. [g] Radiative lifetime, where  $\tau_{\text{rad}} = \tau_{\text{F}}/\Phi_{\text{F}}$ . [h] Band is present as a shoulder or second maximum. [i] Broad high-energy shoulder but no clearly identifiable second maximum.

**Figure 2.** Absorption spectra of BF<sub>2</sub>nbm complexes **1-6** in CH<sub>2</sub>Cl<sub>2</sub>.

The absorptions show a linear dependence on concentration for each of the boron diketonate dyes in CH<sub>2</sub>Cl<sub>2</sub> in the 5–20 μM range. These results suggest that only ground-state monomeric species for **1-6** absorption occur under the tested conditions. The molar extinction coefficients of **1-6** are listed in Table 1. The introduction of bromine atoms to BF<sub>2</sub>n(Br)bm and BF<sub>2</sub>nb(Br)m induces an increase of the extinction coefficients.<sup>28</sup> An anomaly in this trend is when bromides are linked to both sides of the diketone (BF<sub>2</sub>n(Br)b(Br)m; **4**), as the absorption slightly decreased to 34,000 M<sup>-1</sup> cm<sup>-1</sup>. For piperidine complexes **5** and **6**, the extinction coefficient shows a significant, greater than twofold enhancement compared to those of **1-4**, which can also be attributed to the increased electron donor ability of the piperidine unit on the phenyl group.<sup>16,29,30</sup>

The emission spectra of BF<sub>2</sub>nbm complexes **1-6** are provided in Figure 3. We also examined the fluorescence lifetimes of **1-6** in dichloromethane solution. The results are recorded in Table 1. It is widely accepted that heavy atoms can efficiently shorten lifetimes of organic dyes, so it is not surprising that the lifetimes of **2-4**, which contain bromide, have all

dropped.<sup>28,31</sup> However, compared to BF<sub>2</sub>nbm (**1**), BF<sub>2</sub>nb(Br)m (**3**) showed a slight decrease in lifetime, from 4.8 ns to 4.6 ns, whereas the lifetimes of BF<sub>2</sub>n(Br)bm (**2**) and BF<sub>2</sub>n(Br)b(Br)m (**4**) decreased to 0.86 and 0.80, which was about 1/6 of the lifetimes for BF<sub>2</sub>n(Br)bm and BF<sub>2</sub>n(Br)b(Br)m. As previously described, the optical properties of the charge transfer emitting species are dominated by the major donor, naphthyl over phenyl.<sup>16</sup> Therefore, halogen atoms effects are predicted to be stronger when they are attached to naphthyl groups and show little influence when they are substituents on the less powerful arene donors, based on the measured lifetime values. The lifetime measurements of **1-4**, are accurately fit by a single exponential decay, which implies only one excited species existed in each case. However, triple and double exponential decay profiles were required to fit data for BF<sub>2</sub>nb(pip)m (**5**) and BF<sub>2</sub>n(Br)b(pip)m (**6**). This suggests that excited-state twisted isomers may exist for piperidine systems, and that there may be an impact of twisted intramolecular charge transfer (TICT) on the optical properties.<sup>26,32</sup> A near-planar conformation and a more significantly twisted conformation may be accessible to the excited state.<sup>25,33</sup>

**Figure 3.** Normalized emission spectra of BF<sub>2</sub>nbm complexes **1-6** in CH<sub>2</sub>Cl<sub>2</sub> ( $\lambda_{\text{ex}} = 369$  nm).

The quantum yield measurements were carried out with quinine sulfate in 0.1 M H<sub>2</sub>SO<sub>4</sub>. The standard BF<sub>2</sub>nbm dye (**1**) possesses the highest fluorescence quantum yield of 50% ( $\Phi_{\text{F}} = 0.50$ ). Due to the heavy atom effect, the presence of bromide causes the diminished fluorescence via an increased intersystem crossing rate.<sup>34,35</sup> Thus, the quantum yields of **2-4** are all decreased relative to BF<sub>2</sub>nbm. Placement of a single Br on the phenyl fragment reduced the quantum yield to 31%. However, when a bromide is attached on the naphthyl side, the dyes showed more dramatic decreases in quantum yield, to 17% for **2** and 18% for **4**. The quantum yields of piperidyl-substituted phenyl systems **5** and **6** in dichloromethane are ~1.0% and 2.8% respectively. The low quantum yields of **5** and **6** are presumably correlated to strong CT character in the transition which permits large, energy-dissipating nuclear reorganization.<sup>36–38</sup>

**Computational Studies.** To explain the observed optical properties, time-dependent density functional theory (TD-DFT) calculations at the optimized geometries with the model  $\omega$ B97XD/6-311+G(d) and Tomasi solvent provide estimates of S<sub>0</sub>-S<sub>1</sub> absorption (Table 2). The frontier molecular orbital diagrams including highest energy occupied molecular orbitals (HOMOs) and lowest energy unoccupied molecular orbitals (LUMOs) are shown in Figures 4 and 5. The absorption spectra for species **1-6** can be divided into two categories. The phenyl-

## FULL PAPER

WILEY-VCH

piperidyl species, **5** and **6**, absorb at longer wavelengths compared to species **1-4** (450–520 nm or 2.4–2.8 eV for **5** and **6**, 350–425 nm or 2.9–3.5 eV for **1-4**). The phenyl-piperidyl species **5** and **6** absorb more strongly than species **1-4**. Phenyl-piperidyl systems **5** and **6** also have a lower-intensity absorption at 320–350 nm or 3.5–3.9 eV. There is some hint that a second absorption may lie below 300 nm (beyond 4.0 eV) for species **1-4**. The calculated spectra are provided in the Supporting Information (Figures S1–S6).

All features of the experimental spectra are captured by modeling. Computations on species **5** and **6** place the reddest transition at about 3.3 eV, while the computed transition energies for the reddest transitions of species **1-4** lie near 3.6 eV. The singlet TD-DFT calculations seem to have a systematic error, shifting transitions to the blue by roughly 0.4 eV. The greater intensity of absorption for **5** and **6** relative to **1-4** is captured as well. Computed oscillator strengths for **5** and **6** are near 1.7, while for **1-4** the computed oscillator strengths range from 1.1 to 1.5. The variation is associated with the pattern of Br substitution: the unsubstituted species **1** has the smallest oscillator strength. Bromide substitution on naphthyl enhances the oscillator strength more effectively than substitution on the phenyl. The shorter wavelength and weaker band near 3.8 eV clearly evident in the experimental spectra of **5** and **6** is placed at about 3.9 eV in modeling, with oscillator strengths less than 0.05 for both piperidyl-substituted systems. The shorter wavelength (bluer) transitions computed for **1-4** are near 4.0 eV; in contrast to the behavior for the longer wavelength absorption, bromo-substitution on the naphthyl fragment reduces the oscillator strength to ~ 0.15 (**2** and **4**) from ~ 0.25 (**1** and **3**).

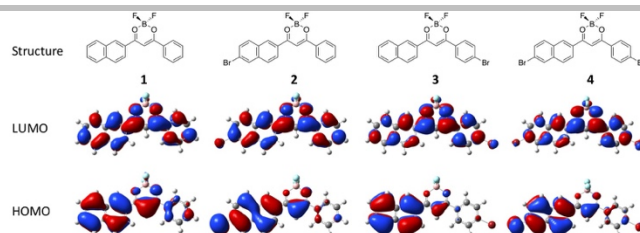


**Figure 4.** Calculated frontier molecular orbital diagrams for compounds **1-4**. Calculated energies are provided in Table S1.

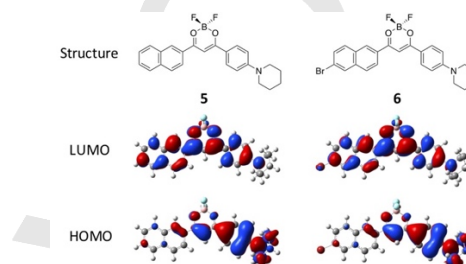


**Figure 5.** Calculated frontier molecular orbital diagrams for **5** and **6**. Calculated energies are provided in Table S1.

**Table 2.** Calculated Energies of Absorption, Fluorescence and Phosphorescence.<sup>[a]</sup>

Sample	Ground State <sup>[b]</sup>		Singlet Excited State <sup>[c]</sup>		Triplet Excited State <sup>[d]</sup>
	S <sub>0</sub> Absorption (eV)	S <sub>0</sub> Absorption (f)	S <sub>1</sub> Emission (eV)	S <sub>1</sub> Emission (f)	T <sub>1</sub> Emission (eV)
<b>1</b>	3.57 4.03 <sup>[e]</sup>	1.09 0.34	3.20 3.89	1.17 0.29	1.73
<b>2</b>	3.64 4.00 <sup>[e]</sup>	1.33 0.14	3.20 3.75	1.47 0.09	1.77
<b>3</b>	3.57 3.87 <sup>[e]</sup>	1.22 0.28	3.18 3.66	1.40 0.17	1.76
<b>4</b>	3.60 3.98 <sup>[e]</sup>	1.46 0.16	3.23 3.77	1.60 0.07	1.74
<b>5</b>	3.23 4.02 <sup>[e]</sup>	1.77 0.04	2.91 3.83	1.88 0.03	1.98
<b>6</b>	3.25 3.98 <sup>[e]</sup>	1.68 0.01	2.94 3.84	1.89 0.05	2.00

[a] Energies and oscillator strengths of dyes 1-6. (See Supporting information for calculated UV/Vis and Cartesian coordinates of all excited states.) [b] Absorption energy (eV) and corresponding oscillator strengths at the optimized ground state geometry. [c] Fluorescence energy (eV) and corresponding oscillator strengths at the optimized singlet excited-state geometry. [d] Phosphorescence energy (eV) and corresponding oscillator strengths at the optimized triplet excited-state geometry. [e] Minor absorption of contributing orbitals.

Calculations provide a pictorial view of the transitions in the absorption spectra, based on the molecular orbital (MO) composition of the excitations. The longest wavelength transitions are almost entirely single excitations from the HOMO to the LUMO. The highest energy occupied MO localized on isolated naphthalene is higher in energy than the highest energy occupied MO on unsubstituted benzene. Bromo- and piperidyl-substitution on such aromatic rings raise the energies of these MOs. Numerical details are provided in Table S1 and accompanying discussion in supplementary material. Piperidyl substitution has a greater effect, so for species **5** and **6** the HOMO is local to the phenyl-piperidyl fragment. In contrast, for **1-4** the HOMO is always local to the naphthyl fragment, regardless of Br substitution. The consequence is that, for the ISC process S<sub>1</sub>→T<sub>1</sub>, Br substitution on naphthyl has only a minor effect on the transitions for **5** and **6**, while Br substitution on naphthyl has a more substantial effect for species **1-4**. Since the phenyl fragment does not participate extensively in the spectra for species **1-4**, Br substitution on phenyl has a less dramatic impact on spectra for these systems.

The red feature in the spectra for **1-3** seems to be composed of two components. We considered the possibility that in solution there may coexist two rotamers, differing in the torsion angle around the bond connecting the naphthyl fragment to the β-diketonate core. The computed energies put these isomers at virtually identical energy (within 0.5 kcal/mol), so an equilibrium between the two forms seems possible. The computed absorption spectra for the two isomers are almost indistinguishable and do not represent the directions of the small shifts in the absorption maxima. These results do not allow us to reach a conclusion on the presence of the two rotamers. The absorption spectrum for **4** seems anomalous. Our modeling suggests the oscillator strength *f* for the red band for **4** should be greater than those values for **1-3**, and we have no explanation for the breadth or shape of this band.

TD-DFT calculations of the emission energies from the lowest excited state for species **1-6** were performed using the optimized excited state geometries. In dichloromethane solution, species **5** and **6** display two emission signals attributed to fluorescence, at about 2.2 and 2.8 eV. The fluorescence quantum yield is very small, and the lifetime for the longer wavelength emission is hardly affected by bromo substitution. For the shorter wavelength emission, bromo substitution halves the fluorescence lifetime. The Stokes shifts, about  $3000\text{ cm}^{-1}$  for the red emission and  $7000\text{ cm}^{-1}$  for the blue emission, are not strongly affected by bromo substitution. Systems **1-4** fluoresce over a range from 2.7 to 2.5 eV. According to the calculations, bromo substitution on the naphthyl fragment shifts the fluorescence to the red, reduces the fluorescence quantum yield, and shortens the fluorescence lifetime. Bromo substitution on phenyl has relatively minor effects. For **1** and **3**, the Stokes shift is about  $4300\text{ cm}^{-1}$  while for **2** and **4** (with bromo substitution on naphthyl) have Stokes shifts of about  $2900\text{ cm}^{-1}$ . The systematic error in modeling excited states is typically greater than the error in describing ground states, and the error in emission properties will be greater than the error for absorption properties. For species **5** and **6** the longer wavelength emissions are predicted to lie at about 2.9 eV, an overestimate of about 0.7 eV. The computed oscillator strengths are large ( $\sim 1.9$ ) and almost identical. With due caution, we observe that the  $S_2-S_0$  energy difference is about 3.8 eV ( $\sim 325\text{ nm}$ ), far from the second experimental feature at 2.8 eV ( $\sim 450\text{ nm}$ ). This transition has a much smaller computed oscillator strength ( $< 0.1$ ) than the  $S_1-S_0$  transition (Table 2).

Modeling of triplet states can be done in two distinct ways. First, the optimized geometry of the triplet can be obtained by direct computation. The  $S_0-T_1$  gap can be estimated by the energy difference between  $S_0$  and  $T_1$  at that geometry (the “ $\Delta$ SCF” method), or by TD-DFT including singlet and triplet excitations from  $S_0$  at the optimized  $T_1$  geometry. Since TD-DFT does not include all energy terms in the SCF calculations, results will differ in principle. In practice, the discrepancy is no more than 0.1 eV. In either case, the predicted phosphorescence energy for **5** and **6** are near 2.0 eV, 620 nm. For **1-4** the computed phosphorescence covers a narrow range from 1.72 to 1.76 eV, with the longer wavelength emissions for **2** and **4**, and the shorter wavelength emissions for **1** and **3**. This is consistent with the effects on spectroscopic features of bromo substitution on the naphthyl fragment seen throughout this discussion. In this case, the systematic error red-shifts the transition by about 0.5 eV, probably because the unrestricted DFT method is more flexible for the triplet than the restricted DFT used for the ground state singlet. Restricted open shell calculations on the triplets may reduce the systematic error.

The lowest triplet orbitals for **2-4** are shown in Figure 6, which are related to the second ISC process, i.e.,  $T_1 \rightarrow S_0$ . From the amplitude distribution in these orbitals, it can be seen that for both **2** and **4**, substantial contribution from the bromine atom can be found for both SOMOs; while for **3**, only one of the SOMOs has significant bromine contribution. The implication is that the radiative decay from the  $T_1$  state will be enhanced more by the heavy atom effect for **2** and **4** than for **3**, given that either SOMO electron spin results in ISC. The results are, in fact, consistent with the fluorescence lifetime data measured in solution, where much shorter lifetimes are seen for **2** and **4**. We can also predict

that the relative intensity ratio of phosphorescence-to-fluorescence ( $I_P/I_F$ ) will be higher for **2** than for **3**.

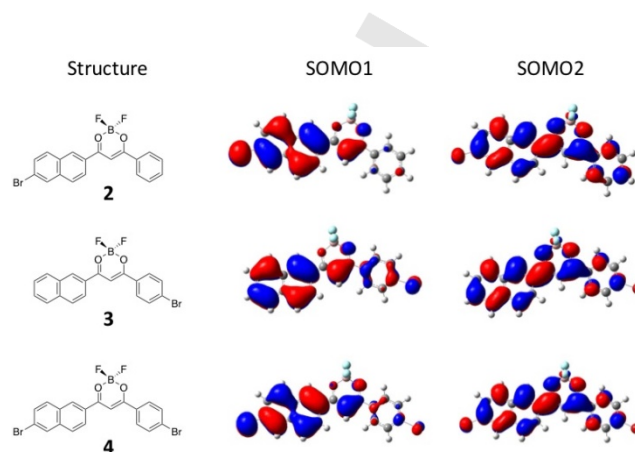


**Figure 6.** Singly occupied molecular orbitals (SOMOs) at the  $T_1$  geometry show that substantial amplitude is found on Br atoms for species **2** and **4**, where the heavy atom substitution is on the naphthyl fragment. In contrast, species **3** has appreciable amplitude on bromine only for one of the SOMOs.

**Optical Properties in PLA Blends.** Dyes were also studied in polymer matrices to activate dual emission, both fluorescence and room temperature phosphorescence. Dyes **1-6** were dispersed in poly(lactic acid) (1.3 weight percent), and the resulting mixture was coated as thin films on vials. Solid-state emission data under air and  $N_2$  are provided in Table 3, and Figures 7 and 8. The fluorescence of compounds **1-4** in PLA showed similar blue emission to dyes in dichloromethane solution. In general, the emission in PLA is slightly blue-shifted versus solution (e.g. **1**  $\lambda_F$  (nm);  $CH_2Cl_2 = 482$ , PLA = 444). This could be linked to the polarity of the environment, as dyes with ICT often show solvatochromism.<sup>39,40</sup> For compounds **5** and **6**, the blue emission disappears. Aggregation in the PLA may induce energy transfer to the lowest energy species.<sup>41,42</sup> Also similar to the pattern of optical properties observed for systems in solution, the fluorescence lifetimes ( $\tau_F$ ) are most greatly influenced by the heavy atom placement. When the bromide is placed on the major donor (**1-4**: naphthyl), the fluorescence lifetimes decrease substantially (e.g.  $\tau_F$  (ns); **1** = 3.29, **2** = 0.78). The increased rate of intersystem crossing depopulates the singlet state, decreasing the fluorescence lifetime.<sup>31</sup>

**Table 3.** Optical Properties of BF<sub>2</sub>nbm Complexes 1-6 in PLA at Room Temperature <sup>[a]</sup>

Sample	$\lambda_F$ <sup>[b]</sup> (nm)	$\lambda_P$ <sup>[c]</sup> (nm)	$\tau_F$ <sup>[d]</sup> (ns)	$\tau_P$ <sup>[e]</sup> (ms)	$I_P/I_F$ <sup>[f]</sup>
1	444	541	3.29	813	0.27
2	437	554	0.78	13.6	0.73
3	449	544	2.52	341	0.44
4	448	561	0.75	12.9	0.80
5	558	580 <sup>[g]</sup>	1.88	[h]	[h]
6	559	[h]	3.46	[h]	[h]

[a] Dye loading: 1.3 wt% in PLA. [b] Fluorescence emission maxima, excited at 369 nm. [c] Phosphorescence emission maxima, excited at 369 nm. [d] Fluorescence lifetimes fitted with single-exponential decay. Excitation source: 369 nm LED monitored at the emission maxima. [e] Room temperature phosphorescence pre-exponential weighted lifetime fit to triple exponential decay. Excitation source: xenon flash lamp. [f] The relative intensity of phosphorescence over fluorescence at the emission maxima under N<sub>2</sub>. [g] Emission maximum estimated from weak broad signal with noise. [h] Signal too weak to be detected.

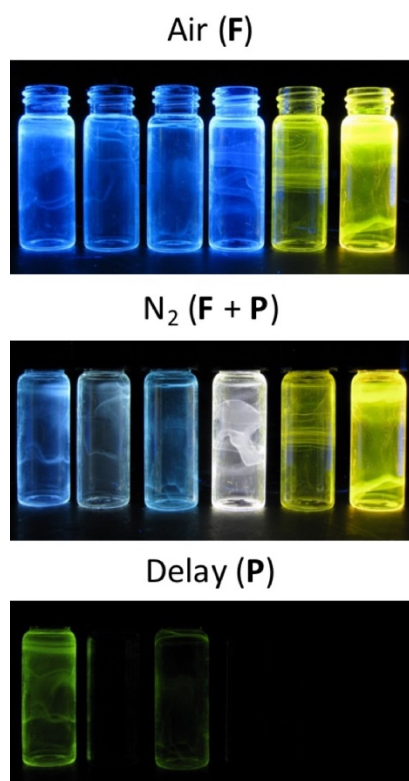


**Figure 7.** Images of dyes 1-6 (in order, left to right) in PLA films inside vials in air (fluorescence), N<sub>2</sub> (fluorescence plus phosphorescence), and under N<sub>2</sub> with the UV source turned off (Delay; phosphorescence) ( $\lambda_{ex} = 369$  nm). Note: Compounds 5 and 6 do not change between air and nitrogen. Dyes 2 and 4 have short lived phosphorescence emissions that are not captured with the camera. Note: The green left edge for sample 2 is a reflection from sample 1.

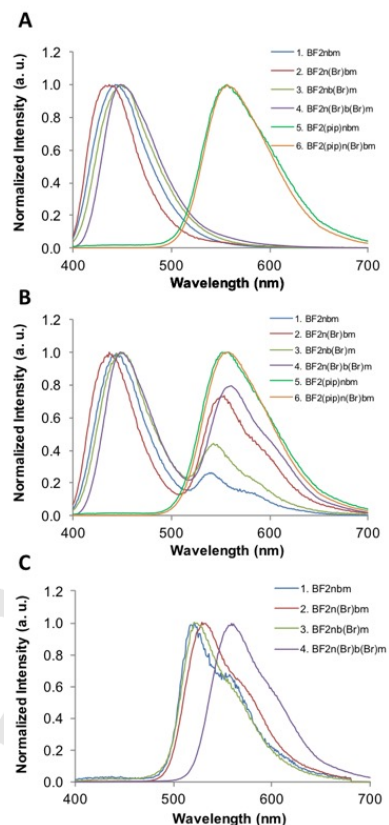


**Figure 8.** Normalized emission spectra BF<sub>2</sub>nbm complexes (1-6) (1.3 wt%) in PLA films ( $\lambda_{ex} = 369$  nm). A) Total emission spectra in air, highlighting fluorescence, with phosphorescence largely quenched by oxygen. B) Total emission spectra under N<sub>2</sub> showing fluorescence and unquenched phosphorescence. C) Delayed emission spectra under N<sub>2</sub> showing phosphorescence (2 ms delay). Note: Total emission of compounds 5 and 6 did not change between air (A) and N<sub>2</sub> (B).

Under N<sub>2</sub>, compounds 1-4 show two emission bands, which correspond to their singlet and triplet emissions, respectively. Dyes BF<sub>2</sub>nb(pip)m and BF<sub>2</sub>n(Br)b(pip)m only showed one emission band which is assigned to the singlet excited state emission. This band showed considerable bathochromic shift compared to singlet emissions of other BF<sub>2</sub>nbm derivatives and is assigned to a charge transfer state. As shown in Table 3, the presence of bromine enhanced the relative phosphorescence intensity in BF<sub>2</sub>n(Br)bm, BF<sub>2</sub>nb(Br)m and BF<sub>2</sub>n(Br)b(Br)m. The relative phosphorescence intensity ( $I_P/I_F$ ) was moderately increased from 0.27 for 1 (BF<sub>2</sub>nbm) to 0.44 for 3 [BF<sub>2</sub>nb(Br)m] when a bromine atom replaced hydrogen on the phenyl group, which is defined as the minor donor in this dye. But when a bromide was attached on the naphthyl group, the relative intensity jumped over two-fold to 0.73 for [BF<sub>2</sub>n(Br)bm]. Introducing an additional bromide on the phenyl unit forming [BF<sub>2</sub>n(Br)b(Br)m], 4, induced only a slight increase to 0.80. Positioning the substituent on the major donor has a dramatic influence on triplet species populations. The heavy atom effect is significantly amplified if the substituent is present on the major electron-donating group. The long lifetime triplet species will be more likely to return to their ground states via either delayed fluorescence or a non-radiative pathway rather than phosphorescence.<sup>43,22,44,45</sup>

The isolated phosphorescence spectra of dyes **1-4** are shown in Figure 8. Dyes **1-3** exhibit phosphorescence with maxima around 540 nm and a shoulder around 560 nm. The phosphorescence emission maximum for BF<sub>2</sub>n(Br)b(Br)m, **4**, is at 559 nm. Compound **5** showed weak phosphorescence, and no obvious phosphorescence was observed for BF<sub>2</sub>n(Br)b(pip)m, **6**. Because there is no significant heavy atom effect in **5** or **6**, the relevant comparisons are with **1** or **3**. If, as the MO diagrams in Figures 4 and 5 suggest, there is greater charge transfer character in the transitions of **5** and **6** than in transitions of **1** and **3**, HOMO and LUMO are more nearly disjoint for **5** and **6**. Then the spin orbit coupling integrals mixing T<sub>1</sub> and S<sub>0</sub> for **5** and **6** would be smaller, and phosphorescence would be weaker. A non-emissive transformation between the twisted and coplanar structures of the aminophenyl moiety could also account for the weak phosphorescence emission.<sup>26</sup>

The phosphorescence lifetimes of dyes **1-4** were also listed in Table 3. We hypothesized that when the groups on both sides of the β-diketonates are not identical, then the group with more electron donating character contributes more to the luminescence properties of the dyes, termed the "major donor" in this report. Modifications on the major donor are expected to show a greater influence on the dye emission properties than substituents on the less important donor. Compound **1**, BF<sub>2</sub>nbm, has the longest triplet state emission lifetime of 813 ms. The lifetimes of Br-substituted **2-4** are all shorter than that of BF<sub>2</sub>nbm. Bromides on the arenes strongly influence the triplet decay lifetimes. The trend matches the pattern of the fluorescence lifetimes in CH<sub>2</sub>Cl<sub>2</sub> solutions. Again, because the naphthyl group is the dominant donor in **1-4**, the modification of naphthyl will lead to a greater change in lifetime. The phosphorescence lifetime of BF<sub>2</sub>n(Br)bm (**2**) was dramatically reduced to 13.6 ms, which is around one sixtieth of that for BF<sub>2</sub>nbm. In comparison, the lifetime of BF<sub>2</sub>nb(Br)m (**3**), with bromide on the phenyl ring, was only decreased to 341 ms. The additional bromide on BF<sub>2</sub>n(Br)b(Br)m (**4**) induced a slight lifetime decrease to 12.9 ms from 13.6 ms for BF<sub>2</sub>n(Br)bm (**2**). These results demonstrate that fluorescence and phosphorescence lifetimes of ICT dyes can be tuned with substituents on aryl electron donors. These are important considerations for tailoring the sensitivity and designing fluorophores for lifetime imaging, such as fluorescence lifetime imaging microscopy and phosphorescence lifetime imaging microscopy (FLIM and PLIM).<sup>46-48</sup> For lifetime-based imaging, sensors like BF<sub>2</sub>nbmPLA,<sup>49-51</sup> a compound with similar properties to compounds **1** and **3** in this study with long phosphorescence lifetimes, can be dynamically quenched by oxygen more quickly, and exhibit a linear response to O<sub>2</sub> within a small range (0.0-0.3% O<sub>2</sub>). The large Stern-Volmer constant makes the sensors sensitive to minor changes in O<sub>2</sub> concentration. This type of sensor may be suitable for measurements in environments depleted of oxygen, such as tumors.<sup>11,52,53</sup> Shorter phosphorescence lifetime sensors such as BF<sub>2</sub>nbm(Br)PLA, analogous to compound (**2**) with a broader linear sensing range (0-3%) are capable of monitoring O<sub>2</sub> in environments more rich in oxygen, such as wounds and tissues.<sup>50</sup>

## Conclusions

From the measurements of quantum yields, triplet state populations and phosphorescence lifetimes of dyes **1-6**, it is concluded that if two donors are present in ICT type fluorophores, the position of the substituted heavy atom, such as a bromine atom in this case, can have substantial effect on the phosphorescence yield. Unlike predominantly local π-π\* transition, charge transfer precludes certain regions and moieties in the molecule from participating in a given electronic transition. Thus, when the heavy atom is precluded, its effect is trivial compared to when it is included. Furthermore, when the heavy atom does participate in the electronic transition, substantial amplitude can be found on it in only one or both SOMOs. This allows for easy modulation of the fluorescence-to-phosphorescence ratio by simply changing the position of heavy atom substitution. For example, comparing **2** and **3**, the bromine on the phenyl ring contributes only to the S<sub>1</sub>→T<sub>1</sub> transition while the bromine on the naphthyl ring contributes both to the S<sub>1</sub>→T<sub>1</sub> and T<sub>1</sub>→S<sub>0</sub> transitions. Consequently, the phosphorescence yield of **2** is visibly higher than that of **3**. The optical properties of BF<sub>2</sub>nb(pip)m (**5**) and BF<sub>2</sub>n(Br)b(pip)m (**6**) seem to depend most strongly on the interaction between piperidinophenyl and difluoroboron. Thus, the modification with bromine on the naphthyl versus phenyl side had little influence on the overall emission due to the exclusion of bromine participation in the electronic transition, which explains the high similarity between BF<sub>2</sub>nb(pip)m and BF<sub>2</sub>n(Br)b(pip)m emissions.

Based on these findings, we can tune the emission properties of ICT dyes either greatly or slightly by introducing substituents on various donors. If the emission properties need to be adjusted only slightly, then substituents can be assigned on minor donors. With substituents on major electron donors, some properties, such as lifetimes, triplet state populations and quantum yields will be greatly affected. These findings may be exploited for the design of oxygen imaging and sensing agents.

## Experimental Section

**Materials.** 3,6-Dimethyl-1,4-dioxane-2,5-dione (D, L-lactide, PURAC Biomaterials, 99.8%) was stored in a drybox under a nitrogen atmosphere and used without further purification. Tin(II) 2-ethylhexanoate (Sn(oct)<sub>2</sub>, Spectrum), ethylene glycol (Sigma-Aldrich, 99.8%), BF<sub>3</sub>·OEt<sub>2</sub> (Sigma-Aldrich, purified and redistilled) and all other reagents were obtained from Sigma-Aldrich and used as received. Anhydrous tetrahydrofuran (THF) and dichloromethane (CH<sub>2</sub>Cl<sub>2</sub>) for reactions were prepared by passage through alumina columns under argon. Poly lactide was prepared as previously described.<sup>54</sup>

**Methods.** <sup>1</sup>H NMR (300 MHz) spectra were recorded on a Varian UnityInova spectrometer in CDCl<sub>3</sub> unless otherwise indicated. Resonances were referenced to the signal for residual protiochloroform at 7.260 ppm. <sup>1</sup>H NMR coupling constants are given in hertz. UV/vis spectra were recorded on a Hewlett-Packard 8452a diode-array spectrophotometer in CH<sub>2</sub>Cl<sub>2</sub>. High resolution mass spectra (HRMS) were obtained with a Micromass Q-TOF Ultima spectrometer using electrospray ionization (ESI). Additional mass spectra were recorded using an Applied Biosystems 4800 spectrometer with a MALDI TOF analyzer. Steady-state fluorescence emission spectra were recorded on a Horiba Fluorolog-3 Model FL3-22 spectrofluorometer (double-grating excitation and double-grating emission monochromators). Phosphorescence spectra were recorded with the same instrument except that a pulsed xenon lamp (λ<sub>ex</sub> = 369 nm; duration < 1 ms) was

used for excitation and spectra were collected with a 1 ms delay after excitation. Time-correlated single-photon counting (TCSPC) fluorescence lifetime measurements were performed with a NanoLED-370 (369 nm) excitation source and DataStation Hub as the SPC controller. Phosphorescence lifetimes were measured with a 500 ns multi-channel scalar (MCS) excited with a pulsed xenon lamp ( $\lambda_{\text{ex}} = 369$  nm; duration < 1 ms). Lifetime data were analyzed with DataStation v2.4 software from Horiba Jobin Yvon. Fluorescence quantum yields,  $\Phi_{\text{F}}$ , for all boron dyes in  $\text{CH}_2\text{Cl}_2$  were calculated versus quinine sulfate in 0.1 M sulfuric acid aqueous solution as a standard using the following values:  $\Phi_{\text{F}}$  quinine sulfate = 0.54,<sup>8</sup>  $n_{\text{D}}^{20} \text{H}_2\text{O} = 1.33$ ,  $n_{\text{D}}^{20} \text{CH}_2\text{Cl}_2 = 1.42$ . Optically dilute  $\text{CH}_2\text{Cl}_2$  solutions of boron diketonates and the 0.1M sulfuric acid quinine sulfate standard solution were prepared in 1 cm path length quartz cuvettes with absorbances  $\approx 0.1$ . Quantum yield measurements were performed with excitation,  $\lambda_{\text{ex}} = 350$  nm, and an emission integration range = 365–695 nm. Boron-dye/PLA blend films were fabricated by a simple casting method: PLA (15 mg, with 1.3 wt% dye content) was dissolved in methylene chloride (3 mL) and a portion of the solution (0.5 mL) was transferred to a borosilicate cover slide and dried *in vacuo* for 10–12 h at RT. The photographs were taken with a Canon Powershot SD890IS Digital Elph camera on the automatic setting (no flash).

**Computational Methods.** We employed a modern functional  $\omega$ B97XD which incorporates range-correction and empirical dispersion,<sup>55</sup> and a flexible Pople basis 6-311+G(d)<sup>56</sup> to compute optimized geometries for the ground singlet state ( $S_0$ ), excited single state ( $S_1$ ) and the lowest energy triplet state ( $T_1$ ). The Tomasi model represented the effects of dichloromethane solvent.<sup>57</sup> Optimization of the lowest singlet excited state was accomplished by use of the time-dependent density functional theory (TD-DFT)<sup>58</sup> and the  $\omega$ B97XD density functional but a smaller Pople basis set 6-31G(d),<sup>59</sup> along with the Tomasi model for dichloromethane. TD-DFT calculations at these optimized geometries with the model  $\omega$ B97XD/6-311+G(d) and Tomasi solvent provide estimates of  $S_0$ - $S_1$  absorption and  $S_1$ - $S_0$  emission frequencies and oscillator strengths for species in solution, and similar calculations incorporating both singlets and triplets give estimates of  $T_1$ - $S_0$  emission energies.

**$\beta$ -Diketone Synthesis: Method A.** The  $\beta$ -diketonate ligands nbm, n(Br)bm, nb(Br)m, n(Br)b(Br)m (**1a-4a**) were prepared by Claisen condensation in the presence of NaH as previously described.<sup>16</sup> A representative synthesis, given for **2a**, is as follows. Acetophenone (400 mg, 3.30 mmol), methyl 6-bromo-2-naphthoate (1.16 g, 4.28 mmol) and THF (20 mL) were added sequentially to a 50 mL round bottom flask. After stirring the mixture for 10 min, a suspension containing sodium hydride (NaH) (125 mg, 4.95 mmol) in THF (10 mL) was added dropwise at room temperature under  $\text{N}_2$ . The mixture was stirred for 20 h before saturated aqueous  $\text{NaHCO}_3$  (1 mL) was added to quench the reaction. THF was removed *in vacuo* before 1 M HCl (20 mL) was added. The aqueous phase was extracted with  $\text{CH}_2\text{Cl}_2$  (3  $\times$  20 mL). The combined organic layers were washed with distilled water (2  $\times$  10 mL) and brine (10 mL), and dried over  $\text{Na}_2\text{SO}_4$  before concentration *in vacuo*. The residue was purified by column chromatography on silica gel eluting with hexanes/ethyl acetate (6:1) to give 6-bromo-2-naphthoyl benzoyl methane as a grey solid (755 mg, 65%). <sup>1</sup>H NMR (300 MHz,  $\text{CDCl}_3$ )  $\delta$  16.92 (s, 1H, COCHCOH), 8.50 (s, 1H, 1'-ArH), 8.06 – 8.02 (m, 4H, 3', 4', 5', 8'-ArH), 7.84 (dd,  $J = 2.7$ ,  $J = 8.7$ , 2H, 2", 6"-ArH), 7.57 – 7.49 (m, 4H, 7', 3", 4", 5"-ArH), 6.98 (s, 1H, COCHCO); MS (MALDI):  $m/z$  calculated for  $\text{C}_{19}\text{H}_{14}\text{BrO}_2$  [M+H]<sup>+</sup> 353.02, found 352.99.

**2-Naphthoyl benzoyl methane, nbm, 1a.** The ligand nbm was prepared by method A but with acetophenone (500 mg, 4.12 mmol), methyl 2-naphthoate (1.03 g, 5.36 mmol) and sodium hydride (167 mg, 6.61 mmol) in THF (40 mL). Column chromatography on silica gel eluting with hexanes/ethyl acetate (6:1) to give 2-naphthoyl benzoyl methane as a pale yellow solid (700 mg, 62%). Data are in accord with the literature.<sup>2</sup>

**2-Naphthoyl 6-bromobenzoyl methane, nb(Br)m, 3a.** The ligand nb(Br)m was prepared by method A, but with 4-bromo acetophenone (1.00 g, 5.00 mmol), methyl 2-naphthoate (1.16 g, 6.03 mmol) and sodium hydride (200 mg, 7.92 mmol) in THF (40 mL). 2-Naphthoyl 6-bromobenzoyl methane was obtained after recrystallization from acetone as a pale yellow solid (968 mg, 55%). <sup>1</sup>H NMR (300 MHz,  $\text{CDCl}_3$ )  $\delta$  16.91 (s, 1H, ArCOH), 8.54 (s, 1H, 1'-ArH), 8.03 – 7.88 (m, 6H, 3', 4', 5', 8', 3", 5"-ArH), 7.66 – 7.53 (m, 4H, 6', 7', 2", 6"-ArH), 6.96 (s, 1H, COCHCO); MS (MALDI):  $m/z$  calculated for  $\text{C}_{19}\text{H}_{14}\text{BrO}_2$  [M+H]<sup>+</sup> 353.02, found 353.00.

**6-Bromo-2-naphthoyl 4-bromobenzoyl methane, n(Br)b(Br)m, 4a.** The ligand n(Br)b(Br)m was prepared by method A, but with 4-bromo acetophenone (626 g, 3.08 mmol), methyl 6-bromo-2-naphthoate (1.00 g, 3.70 mmol) and sodium hydride (117 mg, 4.62 mmol) in THF (40 mL). 6-Bromo-2-naphthoyl 4-bromobenzoyl methane was obtained as a yellow solid after recrystallization (2X) from dichloromethane (675 mg, 51%). <sup>1</sup>H NMR (300 MHz,  $\text{CDCl}_3$ )  $\delta$  16.86 (s, 1H, ArCOH), 8.50 (s, 1H, 1'-ArH), 8.07 (s, 1H, 5'-ArH), 8.03 (dd,  $J = 1.8$ ,  $J = 8.7$ , 1H, 4'-ArH), 7.91 – 7.84 (m, 4H, 3', 8', 3", 5"-ArH), 7.67 – 7.63 (m, 3H, 7', 2", 6"-ArH), 6.94 (s, 1H, COCHCO); MS (MALDI):  $m/z$  calculated for  $\text{C}_{19}\text{H}_{13}\text{Br}_2\text{O}_2$  [M+H]<sup>+</sup> 432.91, found 432.93.

**$\beta$ -Diketone Synthesis: Method B.** The  $\beta$ -diketonate ligands nb(pip)m **5a** and n(Br)b(pip)m **6a** were prepared using lithium diisopropylamide (LDA) instead of NaH as the base. A representative synthesis, given for nb(pip)m **5a**, is as follows. 4-Piperidinoacetophenone (836 mg, 4.00 mmol), methyl 2-naphthoate (891 mg, 4.78 mmol) and THF (20 mL) were added sequentially to a 50 mL round bottom flask. After stirring for 10 min, a solution of lithium diisopropylamide (LDA) (1.73 M in hexanes, 3.00 mL, 6.59 mmol) was added dropwise at -78 °C under  $\text{N}_2$ . The mixture was maintained at -78 °C for 4 h, before it was allowed to warm to room temperature and stirred for an additional 4 h. The reaction was then quenched with saturated aqueous  $\text{NH}_4\text{Cl}$  (10 mL). The aqueous phase was extracted with  $\text{CH}_2\text{Cl}_2$  (3  $\times$  20 mL). The combined organic layers were washed with water twice (2  $\times$  10 mL) and brine (10 mL), and dried over  $\text{Na}_2\text{SO}_4$  before concentration *in vacuo*. The residue was purified by column chromatography on silica gel with hexanes/ethyl acetate (8:1) to give 2-naphthoyl 4-piperidinobenzoyl methane as a brown solid (770 mg, 54%). <sup>1</sup>H NMR (300 MHz,  $\text{CDCl}_3$ )  $\delta$  17.28 (s, 1H, ArCOH), 8.56 (s, 1H, 1'-ArH), 8.06 – 7.91 (m, 6H, 3', 4', 5', 6', 7', 8'-ArH), 7.64 – 7.55 (m, 2H, 2", 6"-ArH), 6.99 – 6.95 (m, 3H, 3", 5"-ArH, COCHCO), 3.42 (m, 4H, 2, 6-piperidino H), 1.72 (s, 6H, 3, 4, 5-piperidino H); MS (MALDI):  $m/z$  calculated for  $\text{C}_{24}\text{H}_{23}\text{NO}_2$  [M]<sup>+</sup> 357.17, found 357.14.

**6-Bromo-2-naphthoyl 4-piperidinobenzoyl methane, n(Br)b(pip)m, 6a.** The ligand n(Br)b(pip)m was prepared by Method B as described above for **5a** but with 4-piperidinoacetophenone (646 mg, 3.08 mmol), methyl 6-bromo-2-naphthoate (1.00 g, 3.70 mmol) and LDA (1.30 M in heptanes/tetrahydrofuran/ethylbenzene, 2.85 mL, 3.70 mmol) in THF (40 mL). Crude 6-bromo-2-naphthoyl 4-piperidinobenzoyl methane obtained after recrystallization from acetone was used for the next step to prepare complex **6** without further purification (968 mg, 55%). Pure **1f** was obtained by hydrolysis of difluoroboron from **6** in methanol.<sup>9</sup> <sup>1</sup>H NMR (300 MHz,  $\text{CDCl}_3$ )  $\delta$  17.22 (s, 1H, ArCOH), 8.48 (s, 1H, 1'-ArH), 8.05 (s, 1H, 5'-ArH), 8.02 (dd,  $J = 1.8$ ,  $J = 8.7$ , 1H, 8'-ArH), 7.95 (d,  $J = 9.0$ , 2H, 2", 6"-ArH), 7.85 – 7.81 (m, 2H, 3', 7'-ArH), 7.62 (dd,  $J = 1.8$ ,  $J = 8.7$ , 1H, 4'-ArH), 6.92 (d,  $J = 9.0$ , 2H, 3", 5"-ArH), 6.89 (s, 1H, COCHCO), 3.39 (m, 4H, 2, 6-piperidino H), 1.68 (s, 6H, 3, 4, 5-piperidino H); MS (MALDI):  $m/z$  calculated for  $\text{C}_{24}\text{H}_{22}\text{BrNO}_2$  [M]<sup>+</sup> 435.08, found 435.06.

**Boron Complex Synthesis. Difluoroboron 2-naphthoyl benzoyl methane, BF<sub>2</sub>nbm, 1.** Boron trifluoride diethyl etherate (88  $\mu\text{L}$ , 0.70 mmol) was added at room temperature under  $\text{N}_2$  to a solution of 2-naphthoyl benzoyl methane **1a** (191 mg, 0.70 mmol) in  $\text{CH}_2\text{Cl}_2$  (20 mL). The mixture was refluxed for 2 h. The precipitate was filtered and recrystallized in acetone to give difluoroboron naphthoyl benzoyl methane as a yellow solid (147 mg, 65%). Data are in accord with the literature.<sup>2</sup>

## FULL PAPER

WILEY-VCH

*Difluoroboron 6-bromo-2-naphthoyl benzoyl methane, BF<sub>2</sub>n(Br)bm, 2.* The same method was employed as for **1**, but with 6-bromo-2-naphthoyl benzoyl methane **2a** (208 mg, 0.59 mmol) and BF<sub>3</sub>·OEt<sub>2</sub> (74 μL, 0.59 mmol) in CH<sub>2</sub>Cl<sub>2</sub> (20 mL). Complex **2** was obtained as a yellow powder after recrystallization in acetone (183 mg, 78%). <sup>1</sup>H NMR (300 MHz, CDCl<sub>3</sub>) δ 8.76 (s, 1H, 1'-ArH), 8.22 (s, 1H, 5'-ArH), 8.20 (m, 1H, 4'-ArH), 8.14 – 8.11 (m, 2H, 3', 8'-ArH), 7.90 (d, 2H, J = 8.7, 2", 6"-ArH), 7.76 – 7.69 (m, 2H, 3", 5"-ArH), 7.62 – 7.57 (m, 2H, 3', 7'-ArH), 7.32 (s, 1H, COCHCO); MS (MALDI): *m/z* calculated for C<sub>19</sub>H<sub>11</sub>BBBrF<sub>2</sub>O<sub>2</sub>Na [M+Na]<sup>+</sup> 422.99. Found 423.03. HRMS (ESI, TOF) *m/z* calculated for C<sub>19</sub>H<sub>12</sub>BBBrF<sub>2</sub>O<sub>2</sub>Na, 422.9979 [M + Na]<sup>+</sup>; found 422.9981.

*Difluoroboron 2-naphthoyl 4-bromobenzoyl methane, BF<sub>2</sub>nb(Br)m, 3.* The same method was followed as for **1**, but with 2-naphthoyl 4-bromobenzoyl methane (191 mg, 0.54 mmol) and BF<sub>3</sub>·OEt<sub>2</sub> (68 μL, 0.54 mmol) in CH<sub>2</sub>Cl<sub>2</sub> (20 mL). Complex **3** was obtained as a yellow powder after recrystallization (2×) in acetone (64 mg, 30%). <sup>1</sup>H NMR (300 MHz, CDCl<sub>3</sub>) δ 8.80 (s, 1H, 1'-ArH), 8.12 – 7.92 (m, 6H, 3', 4', 5', 6', 7', 8'-ArH), 7.75 – 7.61 (m, 4H, 2", 3", 5", 6"-ArH), 7.30 (s, 1H, COCHCO); MS (MALDI): *m/z* calculated for C<sub>19</sub>H<sub>11</sub>BBBrF<sub>2</sub>O<sub>2</sub>Na [M+Na]<sup>+</sup> 422.99. Found 422.96. HRMS (ESI, TOF) *m/z* calculated for C<sub>19</sub>H<sub>12</sub>BBBrF<sub>2</sub>O<sub>2</sub>Na, 422.9979 [M + Na]<sup>+</sup>; found 422.9986.

*Difluoroboron 6-bromo-2-naphthoyl 4-bromobenzoyl methane, BF<sub>2</sub>n(Br)b(Br)m, 4.* The same method was followed as for **1**, but with 6-bromo-2-naphthoyl 4-bromobenzoyl methane (405 mg, 0.94 mmol) and BF<sub>3</sub>·OEt<sub>2</sub> (178 μL, 1.41 mmol) in CH<sub>2</sub>Cl<sub>2</sub> (50 mL). Complex **4** was obtained as a grey powder after recrystallization (3×) in dichloromethane (272 mg, 61%). <sup>1</sup>H NMR (300 MHz, CDCl<sub>3</sub>) δ 8.75 (s, 1H, 1'-ArH), 8.18 – 8.04 (m, 4H, 3', 4', 5', 8'-ArH), 7.91 – 7.88 (d, J = 8.4, 2H, 2", 6"-ArH), 7.75 – 7.72 (d, J = 8.4, 2H, 3", 5"-ArH), 7.28 (s, 1H, COCHCO); MS (MALDI): *m/z* calculated for C<sub>19</sub>H<sub>10</sub>BBBr<sub>2</sub>F<sub>2</sub>O<sub>2</sub>Na [M+Na]<sup>+</sup> 502.90. Found 502.81. HRMS (ESI, TOF) *m/z* calculated for C<sub>19</sub>H<sub>11</sub>BBBr<sub>2</sub>F<sub>2</sub>O<sub>2</sub>Na, 500.9085 [M + Na]<sup>+</sup>; found 500.9106.

*Difluoroboron 2-naphthoyl 4-piperidinobenzoyl methane, BF<sub>2</sub>nb(pip)m, 5.* The same method was followed as for **2**, but with 2-naphthoyl 4-piperidinobenzoyl methane (134 mg, 0.38 mmol) and BF<sub>3</sub>·OEt<sub>2</sub> (118 μL, 0.98 mmol) in CH<sub>2</sub>Cl<sub>2</sub> (30 mL). The crude product was purified with column chromatography (silica gel, hexanes-EtOAc, 2:1) to afford **5** as an orange solid (132 mg, 88%). <sup>1</sup>H NMR (300 MHz, CDCl<sub>3</sub>) δ 8.71 (s, 1H, 1'-ArH), 8.10 – 7.88 (m, 5H, 3', 4', 5', 6', 8'-ArH), 7.65 – 7.54 (m, 3H, 6'-ArH, 2", 6"-ArH), 7.13 (s, 1H, COCHCO), 6.88 (d, J = 9.3, 2H, 3", 5"-ArH), 3.53 (m, 4H, 2, 6-piperidino H), 1.72 (s, 6H, 3, 4, 5-piperidino H); MS (MALDI): *m/z* calculated for C<sub>24</sub>H<sub>22</sub>BF<sub>2</sub>NO<sub>2</sub>Na [M+Na]<sup>+</sup> 428.15. Found 428.10. HRMS (ESI, TOF) *m/z* calculated for C<sub>24</sub>H<sub>23</sub>BF<sub>2</sub>NO<sub>2</sub>, 406.1790 [M + H]<sup>+</sup>; found 406.1801.

*Difluoroboron 6-bromo-2-naphthoyl 4-piperidinobenzoyl methane BF<sub>2</sub>n(Br)b(pip)m, 6.* The same method was used as for **2**, but with 6-bromo-2-naphthoyl 4-piperidinobenzoyl methane (106 mg, 0.24 mmol) and BF<sub>3</sub>·OEt<sub>2</sub> (31 μL, 0.24 mmol) in CH<sub>2</sub>Cl<sub>2</sub> (50 mL). Complex **6** was obtained as an orange solid after recrystallization in acetone (65 mg, 56%). <sup>1</sup>H NMR (300 MHz, CDCl<sub>3</sub>) δ 8.67 (s, 1H, 1'-ArH), 8.10 – 8.04 (m, 4H, 3', 4', 5', 8'-ArH), 7.85 (dd, J = 6.3, J = 8.7, 2H, 2", 6"-ArH), 7.65 (dd, J = 1.8, J = 9.2, 1H, 6'-ArH), 7.10 (s, 1H, COCHCO), 6.88 (d, J = 9.3, 2H, 3", 5"-ArH), 3.54 (m, 4H, 2, 6-piperidino H), 1.73 (s, 6H, 3, 4, 5-piperidino H); MS (MALDI): *m/z* calculated for C<sub>24</sub>H<sub>21</sub>BBBrF<sub>2</sub>NO<sub>2</sub>Na [M+Na]<sup>+</sup> 506.06. Found 506.10. HRMS (ESI, TOF) *m/z* calculated for C<sub>24</sub>H<sub>22</sub>BBBrF<sub>2</sub>NO<sub>2</sub>, 484.0895 [M + H]<sup>+</sup>; found 484.0906.

## Acknowledgements

This research was supported by the National Science Foundation (CHE 0718879, CHE 1213915) and the National Cancer Institute of the National Institutes of Health under the

grant number R01CA167250. The Goldwater Scholarship Foundation is acknowledged for a fellowship to Ruffin E. Evans. The research fund BABKO of Marmara University provided support to Zikri Altun. We thank Nguyen D. Nguyen and Alan D. Chien for their assistance, and Prof. J. N. Demas for helpful discussions.

**Keywords:** Boron Complexes • Phosphorescence • Heavy Atom • Charge Transfer • Oxygen Sensing

## References

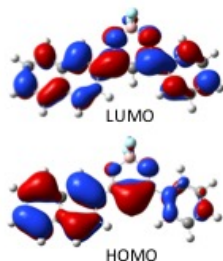
- [1] X. Wang, O. S. Wolfbeis, *Chem. Soc. Rev.* **2014**, *43*, 3666–3761.
- [2] Y. Kajiwara, A. Nagai, K. Tanaka, Y. Chujo, *J. Mater. Chem. C* **2013**, *1*, 4437–4444.
- [3] D. Fyfe, *Nat. Photonics* **2009**, *3*, 453–455.
- [4] S. Mukherjee, P. Thilagar, *Chem. Commun.* **2015**, *51*, 10988–1003.
- [5] O. Bolton, K. Lee, H.-J. Kim, K. Y. Lin, J. Kim, *Nat. Chem.* **2011**, *3*, 205–210.
- [6] Z. An, C. Zheng, Y. Tao, R. Chen, H. Shi, T. Chen, Z. Wang, H. Li, R. Deng, X. Liu, et al., *Nat. Mater.* **2015**, *14*, 685–690.
- [7] G. Zhang, J. Chen, S. J. Payne, S. E. Kooi, J. N. Demas, C. L. Fraser, *J. Am. Chem. Soc.* **2007**, *129*, 8942–8943.
- [8] C. Wu, B. Bull, K. Christensen, J. McNeill, *Angew. Chem. Int. Ed.* **2009**, *48*, 2741–2745.
- [9] X. Wang, H. H. Gorris, J. A. Stolwijk, R. J. Meier, D. B. M. Groegel, J. Wegener, O. S. Wolfbeis, *Chem. Sci.* **2011**, *2*, 901–906.
- [10] G. Zhang, S. E. Kooi, J. N. Demas, C. L. Fraser, *Adv. Mater.* **2008**, *20*, 2099–2104.
- [11] M. Hockel, P. Vaupel, *JNCI J. Natl. Cancer Inst.* **2001**, *93*, 266–276.
- [12] G. Zhang, G. M. Palmer, M. W. Dewhirst, C. L. Fraser, *Nat. Mater.* **2009**, *8*, 747–751.
- [13] J. Liu, W. Bu, J. Shi, *Chem. Rev.* **2017**, *117*, 6160–6224.
- [14] R. Weissleder, *Nat. Biotechnol.* **2001**, *19*, 316–317.
- [15] X. Zhang, T. Xie, M. Cui, L. Yang, X. Sun, J. Jiang, G. Zhang, *ACS Appl. Mater. Interfaces* **2014**, *6*, 2279–2284.
- [16] S. Xu, R. E. Evans, T. Liu, G. Zhang, J. N. Demas, C. O. Trindle, C. L. Fraser, *Inorg. Chem.* **2013**, *52*, 3597–3610.
- [17] C. A. DeRosa, M. Kolpaczynska, C. Kerr, M. L. Daly, W. A. Morris, C. L. Fraser, *ChemPlusChem* **2016**, *82*, 399–406.
- [18] C. A. DeRosa, J. Samonina-Kosicka, Z. Fan, H. C. Hendargo, D. H. Weitzel, G. M. Palmer, C. L. Fraser, *Macromolecules* **2015**, *48*, 2967–2977.
- [19] J. Samonina-Kosicka, C. A. DeRosa, W. A. Morris, Z. Fan, C. L. Fraser, *Macromolecules* **2014**, *47*, 3736–3746.
- [20] X. Chen, C. Xu, T. Wang, C. Zhou, J. Du, Z. Wang, H. Xu, T. Xie, G. Bi, J. Jiang, et al., *Angew. Chem. Int. Ed.* **2016**, *55*, 9872–9876.
- [21] X. Sun, B. Zhang, X. Li, C. O. Trindle, G. Zhang, *J. Phys. Chem. A* **2016**, *120*, 5791–5797.
- [22] Z. Yang, Z. Mao, Z. Xie, Y. Zhang, S. Liu, J. Zhao, J. Xu, Z. Chi, M. P. Aldred, *Chem. Soc. Rev.* **2017**, *46*, 915–1016.
- [23] S. Y. Lee, T. Yasuda, Y. S. Yang, Q. Zhang, C. Adachi, *Angew. Chem. Int. Ed.* **2014**, *126*, 6520–6524.
- [24] H.-W. Mo, Y. Tsuchiya, Y. Geng, T. Sagawa, C. Kikuchi, H. Nakanotani, F. Ito, C. Adachi, *Adv. Funct. Mater.* **2016**, *26*, 6703–6710.
- [25] Z. R. Grabowski, K. Rotkiewicz, W. Rettig, *Chem. Rev.* **2003**, *103*, 3899–4032.
- [26] Y. Kubota, Y. Sakuma, K. Funabiki, M. Matsui, *J. Phys. Chem. A* **2014**, *118*, 8717–8729.
- [27] J. Hu, Z. He, Z. Wang, X. Li, J. You, G. Gao, *Tetrahedron Lett.* **2013**, *54*, 4167–4170.
- [28] W. A. Morris, T. Liu, C. L. Fraser, *J. Mater. Chem. C* **2015**, *3*, 352–363.
- [29] M. J. Mayoral, P. Ovejero, M. Cano, G. Orellana, *Dalton Trans.* **2011**, *40*, 377–383.

- [30] Y. N. Kononevich, I. B. Meshkov, N. V. Voronina, N. M. Surin, V. A. Sazhnikov, A. A. Safonov, A. A. Bagaturyants, M. V. Alfimov, A. M. Muzafarov, *Heteroat. Chem.* **2013**, *24*, 271–282.
- [31] C. A. DeRosa, C. Kerr, Z. Fan, M. Kolpaczynska, A. S. Mathew, R. E. Evans, G. Zhang, C. L. Fraser, *ACS Appl. Mater. Interfaces* **2015**, *7*, 23633–23643.
- [32] S. Sasaki, G. P. C. Drummen, G. Konishi, *J. Mater. Chem. C* **2016**, *4*, 2731–2743.
- [33] J. B. Grimm, B. P. English, J. Chen, J. P. Slaughter, Z. Zhang, A. Revyakin, R. Patel, J. J. Macklin, D. Normanno, R. H. Singer, et al., *Nat. Methods* **2015**, *12*, 244–250.
- [34] S. K. Lower, M. A. El-Sayed, *Chem. Rev.* **1966**, *66*, 199–241.
- [35] W. A. W. A. Morris, M. Sabat, T. Butler, C. A. DeRosa, C. L. Fraser, *J. Phys. Chem. C* **2016**, *120*, 14289–14300.
- [36] Y. Mizuno, Y. Yisilamu, T. Yamaguchi, M. Tomura, T. Funaki, H. Sugihara, K. Ono, *Chemistry* **2014**, *20*, 13286–13295.
- [37] A. Felouat, A. D'Aléo, A. Charaf-Eddin, D. Jacquemin, B. Le Guennic, E. Kim, K. J. Lee, J. H. Woo, J.-C. Ribierre, J. W. Wu, et al., *J. Phys. Chem. A* **2015**, *119*, 6283–6295.
- [38] A. Hirose, K. Tanaka, R. Yoshii, Y. Chujo, *Polym. Chem.* **2015**, *6*, 5590–5595.
- [39] A. Marini, A. Munnoz-Losa, A. Biancardi, B. Mennucci, A. Muñoz-Losa, A. Biancardi, B. Mennucci, *J. Phys. Chem. B* **2010**, *114*, 17128–17135.
- [40] T. Butler, W. A. Morris, J. Samonina-Kosicka, C. L. Fraser, *ACS Appl. Mater. Interfaces* **2016**, *8*, 1242–1251.
- [41] X. Li, H. Liu, X. Sun, G. Bi, G. Zhang, *Adv. Opt. Mater.* **2013**, *1*, 549–553.
- [42] X. Sun, X. Zhang, X. Li, S. Liu, G. Zhang, *J. Mater. Chem.* **2012**, *22*, 17332–17339.
- [43] M. L. Daly, C. A. DeRosa, C. Kerr, W. A. Morris, C. L. Fraser, *RSC Adv.* **2016**, *6*, 81631–81635.
- [44] J. Li, Y. Qian, L. Xie, Y. Yi, W. Li, W. Huang, *J. Phys. Chem. C* **2015**, *119*, 2133–2141.
- [45] R. Ghosh, D. K. Palit, *J. Phys. Chem. A* **2015**, *119*, 11128–11137.
- [46] E. Baggaley, S. W. Botchway, J. W. Haycock, H. Morris, I. V. Sazanovich, J. a. G. Williams, J. a. Weinstein, *Chem. Sci.* **2014**, *5*, 879–886.
- [47] R. I. Dmitriev, S. M. Borisov, A. V. Kondrashina, J. M. P. Pakan, U. Anilkumar, J. H. M. Prehn, A. V. Zhdanov, K. W. McDermott, I. Klimant, D. B. Papkovsky, *Cell. Mol. Life Sci.* **2014**, 367–381.
- [48] M. K. Kuimova, G. Yahioglu, J. A. Levitt, K. Suhling, *J. Am. Chem. Soc.* **2008**, *130*, 6672–6673.
- [49] A. S. Mathew, C. A. DeRosa, J. N. Demas, C. L. Fraser, *Anal. Methods* **2016**, *8*, 3109–3114.
- [50] C. A. DeRosa, S. A. Seaman, A. S. Mathew, C. M. Gorick, Z. Fan, J. N. Demas, S. M. Peirce, C. L. Fraser, *ACS Sens.* **2016**, *1*, 1366–1373.
- [51] S. J. Payne, G. Zhang, J. N. Demas, C. L. Fraser, B. A. Degraff, *Appl. Spectrosc.* **2011**, *65*, 1321–1324.
- [52] X. Zheng, X. Wang, H. Mao, W. Wu, B. Liu, X. Jiang, *Nat Commun* **2015**, *6*, 5834.
- [53] X. Zheng, H. Tang, C. Xie, J. Zhang, W. Wu, X. Jiang, *Angew. Chem. Int. Ed.* **2015**, *127*, n/a-n/a.
- [54] G. Zhang, S. Xu, A. G. Zestos, R. E. Evans, J. Lu, C. L. Fraser, *ACS Appl. Mater. Interfaces* **2010**, *2*, 3069–3074.
- [55] J.-D. Chai, M. Head-Gordon, *Phys. Chem. Chem. Phys.* **2008**, *10*, 6615–6620.
- [56] R. Krishnan, J. S. Binkley, R. Seeger, J. A. Pople, *J. Chem. Phys.* **1980**, *72*, 650–654.
- [57] R. Tomasi, J.; Mennucci, B.; Cammi, J. Tomasi, B. Mennucci, R. Cammi, *Chem. Rev.* **2005**, *105*, 2999–3094.
- [58] F. Furche, R. Ahlrichs, *J. Chem. Phys.* **2002**, *117*, 7433–7447.
- [59] M. S. Gordon, J. S. Binkley, J.A. Pople, W. Pietro, W. J. Hehre, *Chem. Soc.* **1982**, *104*, 2797–2803.

## Entry for the Table of Contents

## FULL PAPER

## Theory



## Oxygen Sensing



Tiandong Liu, Prof. Dr. Guoqing Zhang, Ruffin E. Evans, Prof. Dr. Carl O. Trindle, Prof. Dr. Zikri Altun, Prof. Dr. Christopher A. DeRosa, Fang Wang, Meng Zhuang, and Prof. Dr. Cassandra L. Fraser\*

Page No. – Page No.

**Phosphorescence Tuning via Heavy Atom Placement in Unsymmetrical Difluoroboron  $\beta$ -Diketonate Materials**